JOURNAL OF MAGNETIC RESONANCE **133,** 236–240 (1998)
ARTICLE NO. MN981457

Measurement of Carbon–Phosphorus *J* Coupling Constants in RNA Using Spin–Echo Difference Constant-Time HCCH–COSY

Charles G. Hoogstraten and Arthur Pardi[1]

Department of Chemistry and Biochemistry, Campus Box 215, University of Colorado, Boulder, Boulder, Colorado 80309

Received October 24, 1997; revised March 19, 1998

We report a novel NMR technique for the measurement of carbon–phosphorus coupling constants in RNA oligomers. This method, spin–echo difference constant-time HCCH–COSY, takes advantage of the well-dispersed H1′ and C1′ resonances to analyze couplings involving the more poorly dispersed ribose carbon and phosphorus resonances. The technique was applied to analysis of the $^3J_{C2'P}$ coupling constants related to backbone ϵ torsion angles in a 30-nucleotide lead-dependent ribozyme. $^3J_{C2'P}$ coupling constants were obtained for ~90% of the residues in this RNA, which is over twice as many as could be obtained with previous methods.

Key Words: J **coupling constants; lead-dependent ribozyme; nuclear magnetic resonance; quantitative** *J* **correlation; RNA structure.**

The data for an NMR solution structure determination of a biological macromolecule consist of NOE cross peaks, indicating pairs of protons that are close in space, and three-bond scalar (*J*) coupling constants, which are related to torsion angles via the appropriate Karplus relations (*1*). In RNA oligomers, three-bond $^3J_{HH}$, $^3J_{HC}$, $^3J_{HP}$, and $^3J_{CP}$ couplings provide information on the backbone torsion angles that define the local structure of the molecule (*2–4*). Analysis of the cross peaks in COSY-type spectra can be used to determine *J* values in very short RNAs, but this method fails in larger molecules due to the overlap of multiplet components. The poor dispersion and inefficient transfer properties of the ^{31}P resonances in RNA pose particular difficulties in the measurement of J_{HP} and J_{CP} coupling constants. In some cases, these couplings may be analyzed by the FIDS multiplet-fitting technique (*5, 6*). E.COSY-based methods (*7*) are less sensitive to overlap than multiplet analysis and have been applied to RNAs, notably for $^3J_{HH}$ measurement (*5, 8, 9*), but are not easily applicable to coupling constants involving phosphorus due to the lack of a large, conformation-independent coupling to separate the E.COSY peak components.

Recently, Bax and co-workers (*10*) developed a new methodology for coupling constant determination that operates by measurement of peak intensities in *J*-modulated spectra rather than by analysis of component separation. This principle allows measurement of *J* coupling constants that are inaccessible by other techniques. In the simplest case, the method involves free precession for a fixed period on one of the nuclei involved in the coupling to be measured. Two spectra are taken, one in which the *J* coupling of interest is active during this period and the other in which this *J* coupling is inactive. Peak intensities in the coupled spectrum will be attenuated by a factor of $\cos(\pi JT)$, where *J* is the coupling of interest and *T* is the fixed delay. The desired *J* value can then be easily extracted from the ratio of the intensities in the two spectra. Because the coupling is derived from peak intensities, overlap of multiplet components does not interfere with the analysis.

We have previously reported the adaptation of the spin–echo difference constant-time HSQC (CT–HSQC) experiment (*11*), an example of this methodology, to the measurement of $^3J_{CP}$ couplings in RNA oligomers (*12*). In this experiment, the $^3J_{C2'P}$ coupling constants, which are related to the C2′–C3′–O3′–P (ϵ) torsion angle, were measured by analysis of the *J* modulation of the C2′ resonances. For canonical A-form RNA, the trans ϵ rotamer predicts $^3J_{C2'P}$ values less than ~3 Hz, whereas gauche$^-$ rotamers predict couplings of 8–12 Hz, and the gauche$^+$ rotamer for ϵ is sterically unfavorable (*2*). Unfortunately, this experiment is seriously handicapped by overlap in the poorly resolved H2′/C2′ region of the CT–HSQC spectrum. For example, in the 30-nucleotide RNA oligomer used in these experiments, only 12 of the 29 possible $^3J_{C2'P}$ couplings could be analyzed in CT–HSQC spectra due to poor dispersion of the C2′ and H2′ resonances (*12*), and therefore only a small number of the ϵ torsion angles in the molecule could be determined.

In this report, we take advantage of the superior dispersion of H1′ and C1′ resonances in RNA to enormously improve the analysis of $^3J_{C2'P}$ values in RNA. This is accomplished using a novel three-dimensional (3D) pulse sequence, spin–echo difference CT–HCCH–COSY, that gives dramatically reduced peak overlap. This experiment is implemented on the leadzyme (LZ2), an *in vitro*-selected 30-nucleotide lead-dependent catalytic RNA that has been well-studied by NMR (*13–17*) (Fig. 1).

The pulse sequences used in this work are described in Fig. 2. The sequences are derivatives of the HCCH–COSY exper-

[1] To whom correspondence should be addressed. Fax: (303) 492-2439. E-mail: arthur.pardi@colorado.edu.

1090-7807/98 $25.00

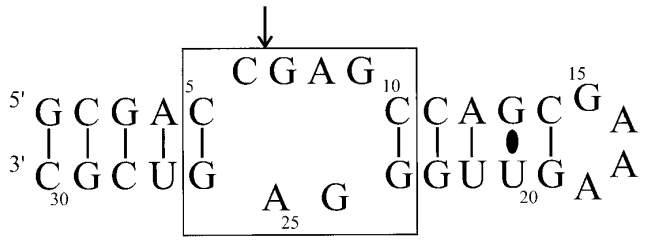

FIG. 1. Secondary structure of LZ2, the lead-dependent ribozyme used in this paper. The autocleavage site is indicated with an arrow and the active-site internal loop is boxed.

iment (*18*), which transfers proton magnetization to the directly bound carbon using INEPT, then to adjacent carbon(s) using a ^{13}C–^{13}C COSY pulse, and back to proton for detection using reverse INEPT. In the present implementation, the transfer pathway is H1′ → uC1′ → uC2′ → uH2′. Incremented evolution may occur on either carbon for this 3D sequence, and the versions with labeling of the C2′ and C1′ resonances are shown in Figs. 2A and 2B, respectively; the following discussion is specific to Fig. 2A. Following ^{1}H frequency labeling during t_1, $-C1'_yH1'_z$ magnetization created at b by the INEPT sequence evolves into $C1'_yC2'_z$ and is converted to $-C1'_zC2'_y$ magnetization by the ^{13}C–^{13}C COSY pulse at c. Since the delay between c and d is set to a multiple of $1/J_{CC}$ (see below), the carbon coherence will not refocus with respect to adjacent carbon atoms. Therefore, a selective pulse is applied to the C1′ region to allow the C1′–C2′ coupling between points c and d to evolve by an odd multiple of $1/2J_{CC}$, resulting in a selective refocusing of the desired coherence to $C2'_yH2'_z$ prior to the reverse INEPT sequence beginning at d. The second selective pulse, at the very end of the constant-time delay, corrects for phase artifacts introduced by the first selective pulse (*19*). Magnetization is finally detected on H2′ during t_3. The C2′ precession period (c–d) is adjusted to a multiple of $1/J_{CC}$ to refocus C2′ magnetization with respect to C3′, with $2/J_{CC}$ the best choice for J_{CP} coupling constants less than ~5 Hz. The highly selective nature of the transfers allows the reduction of the sweep widths in the indirect dimensions (see figure legends). The placement and phases of ^{31}P inversion pulses result in J_{CP} couplings being either active or inactive during the constant-time delay (see figure legend), and the ^{31}P-coupled and -decoupled spectra are collected in interleaved fashion. The constant-time C1′-evolution sequence (Fig. 2B) differs only in the detailed timing of particular delays and in the means employed to achieve ^{31}P-decoupling.

We have implemented the spin-echo difference CT–HCCH–COSY experiment on a 1.2 mM 99% ^{13}C, ^{15}N-labeled sample of LZ2 in D_2O, synthesized as previously described (*17, 20*). A constant-time delay of 47 ms was used, which was optimized by determining the time that resulted in a null spectrum in the C2′ region for a pulse sequence omitting the C1′-selective pulses. (This value yields an estimate of 42.5 Hz for the $^{1}J_{C1'C2'}$ coupling constant.) Spectra were collected and analyzed in both the H1′–C2′–H2′ and H1′–C1′–H2′ formats corresponding to the pulse sequences of Figs. 2A and 2B, respectively.

The greater dispersion of the H1′ resonances in RNA results in a well-resolved CT–HCCH–COSY spectrum and therefore, for larger RNA oligomers, allows a significant increase in the number of residues for which $^{3}J_{C2'P}$ coupling constants can be determined. Figure 3 compares the H2′–C2′ region of the 2D ^{31}P-decoupled CT–HSQC spectrum of LZ2 reported by Legault *et al.* (*12*) to planes at particular H1′ chemical shifts through the 3D ^{31}P-decoupled H1′–C2′–H2′ CT–HCCH–COSY spectrum. The severe overlap in the CT–HSQC spectrum is clearly visible. The CT–HCCH–COSY spectrum, by contrast, allows analysis of almost all residues in LZ2; only U27 and C28, which have unresolved chemical shifts for H1′, C1′, C2′, and H2′, could not be analyzed. Coupling constants determined from both versions of the CT–HCCH–COSY experiment, along with values from Legault *et al.* (*12*) for comparison, are shown in Table 1. For 15 of the residues in LZ2, CT–HCCH–COSY spectra provided useful data on the value of $^{3}J_{C2'P}$, whereas the CT–HSQC experiment failed completely due to peak overlap. Couplings were extracted from measured peak heights using the relationship $I_c/I_d = \cos(\pi JT)$, where I_c is the intensity in the coupled spectrum, I_d is the intensity in the decoupled spectrum, and T is the constant-time delay, as previously described (*12*). Since, for A-form RNA, $^{3}J_{C2'P}$ is very close to zero (*2*), error estimates were obtained by analysis of the deviations of I_c/I_d from unity for residues in regions of known A-form structure. This procedure is justified by the observation of approximately equal numbers of positive and negative deviations from unity for these residues in both spectra. Nonzero values of $^{3}J_{C2'P}$ for these residues would yield an overestimate of the experimental error; therefore, this procedure will not lead to unjustified precision in reported couplings.

For the CT–HCCH–COSY experiment, carbon chemical-shift evolution may proceed on either C2′ or C1′. We have performed and analyzed both types of experiments in LZ2 (Table 1). Evolution on C2′ provides a conceptually simple generalization of the CT–HSQC spectrum by spreading the C2′/H2′ correlations into the third dimension using H1′, whereas C1′ evolution often provides better resolution by taking advantage of the improved dispersion of C1′ compared to C2′ resonances in RNA. Figure 3 shows the C2′-evolution version, which allows direct comparisons with the 2D CT–HSQC data. Figure 3D illustrates an atypical case in which C2′ evolution yields superior peak dispersion to C1′ evolution, since G13 and G23 have identical C1′ chemical shifts but are cleanly separated in the H1′–C2′–H2′ spectrum.

In spin-echo difference CT–HCCH–COSY, couplings are extracted from a comparison of peak intensities in two spectra. Ideally, in such cases, two sets of internal control peaks should

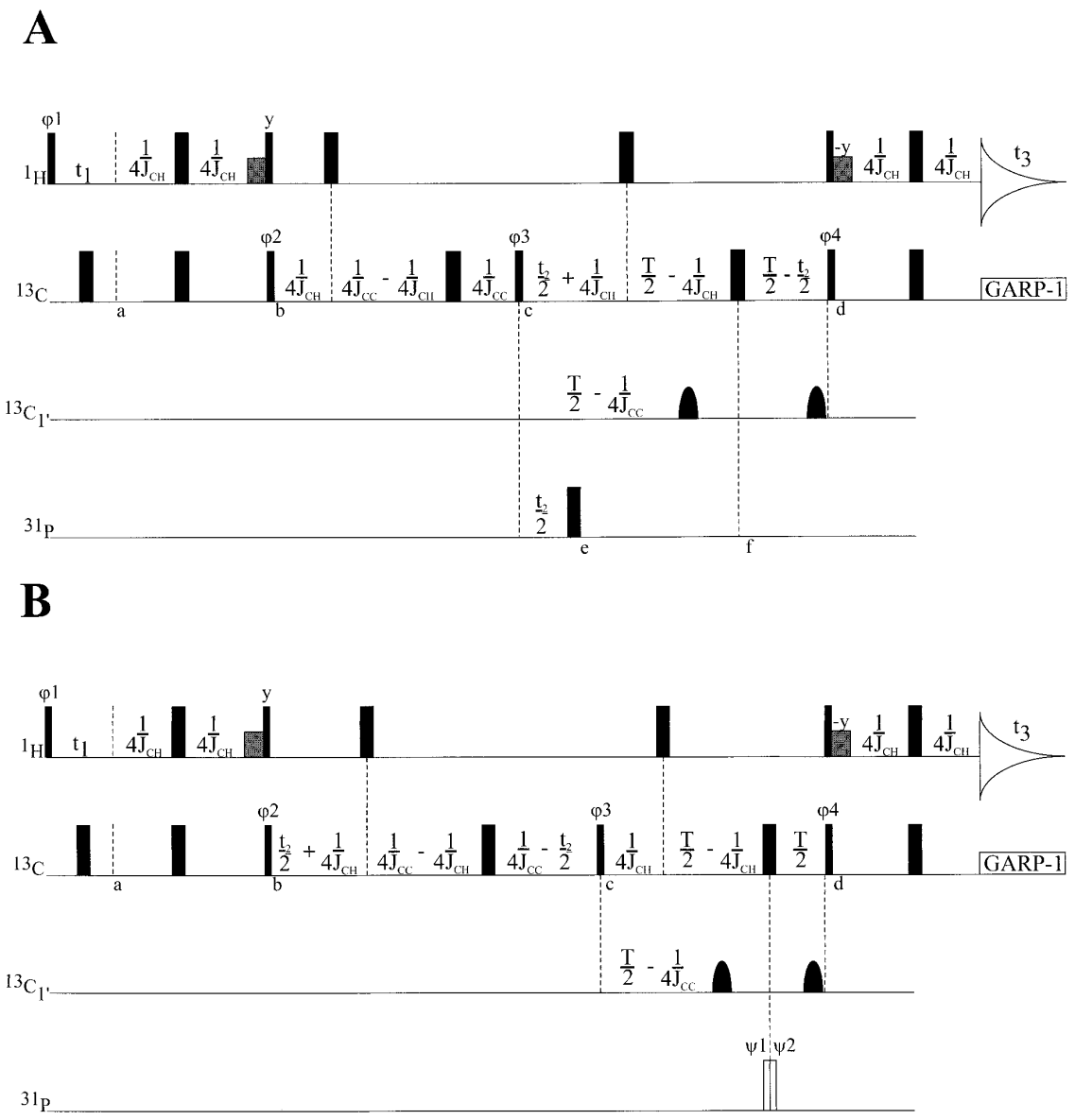

FIG. 2. Pulse sequence for spin–echo difference CT–HCCH–COSY with ^{13}C evolution on (A) C2′ and (B) C1′, 90° and 180° RF pulses are indicated by narrow and wide rectangles, respectively. Shaded rectangles are extended pulses to eliminate unwanted coherences (*26*). This pulse sequence could be further enhanced with *z*-gradient pulses arranged for coherence destruction (*27*); for the probe used for most of this work, gradients were not available. Shaped pulses represent band-selective pulses tuned to invert the C1′ spectral region. Phase cycle: $\phi 1$, $x, -x$; $\phi 2$, $x, x, -x, -x$; $\phi 3$: $x, x, x, x, -x, -x, -x, -x$; $\phi 4$, x; receiver, $x, -x, -x, x$. Other phases are x unless otherwise indicated. Quadrature detection is obtained via the States–TPPI scheme (*28*) with incrementation of $\phi 1$ for t_1 and $\phi 4$ for t_2 (C2′ evolution) or $\phi 1$ for t_1 and $\phi 2$ for t_2 (C1′ evolution). In the C2′-evolution version, the ^{31}P-decoupled spectrum is illustrated; for the ^{31}P-coupled spectrum, the ^{31}P inversion pulse at e is replaced by an equivalent pulse applied at *f*. For the C1′-evolution version, $\psi_1 = x$ and $\psi_2 = -x$ for the ^{31}P-decoupled spectrum, whereas $\psi_1 = \psi_2 = x$ for the ^{31}P-coupled spectrum. For the spectra of LZ2 reported here, delays of $1/4J_{CH} = 1.5$ ms, $1/4J_{CC} = 5.7$ ms, and $T = 47$ ms were used. A ^1H carrier frequency of 4.76 ppm with sweep widths of 6000 Hz in t_3 and 1500 Hz in t_1 was used. A ^{13}C carrier frequency of 79 ppm with a sweep width of 2250 Hz and 56 complex points in t_2, 58 complex points in t_1, and 8 transients per increment was used for the C2′-evolution spectra. For the C1′-evolution spectra, a ^{13}C carrier frequency of 86 ppm with a sweep width of 3000 Hz and 32 complex points in t_2, 36 complex points in t_1, and 16 transients per increment was used. ^{31}P-decoupled and -coupled spectra were acquired in interleaved fashion. Total experimental times were 118 h (CT–C2′) and 82 h (CT–C1′). Selective inversion of the C1′ region was obtained with a 3.5-ms IBURP2 (*29*) pulse applied at 92.4 ppm. ^{13}C decoupling during t_3 was obtained using GARP-1 (*30*) at a power of 1140 Hz. All spectra were obtained at 25°C on a Varian UnityPlus or Unity INOVA 500 MHz spectrometer using Nalorac $^1H\{^{13}C, ^{31}P\}$ or $^1H\{^{13}C, ^{15}N, ^{31}P\}$ probes.

be available; one corresponding to zero coupling, for which the intensities in the two spectra will be identical within noise ($I_c/I_d \sim 1$), and one corresponding to large and known coupling values, for which the coupled spectrum will be substantially attenuated ($I_c/I_d \ll 1$). In the CT–HSQC technique these two types of controls are provided by C1′ resonances, which have

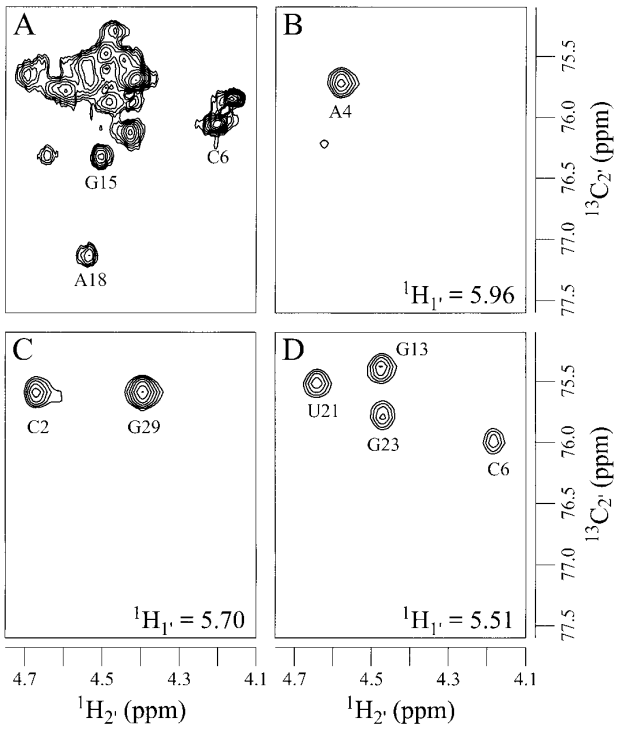

FIG. 3. Comparison of the H2′–C2′ region of (A) a ^{31}P-decoupled CT–HSQC spectrum with (B–D) three planes perpendicular to the H1′ axis of a ^{31}P-decoupled, H1′–C2′–H2′ CT–HCCH–COSY spectrum. The CT–HSQC was acquired and processed as described in Legault *et al.* (*12*). The CT–HCCH–COSY was acquired as described in the legend to Fig. 2A and processed to a final matrix of 2048 × 256 × 128 (data outside the central 1500 Hz window in ω_3 were discarded) using 3-Hz exponential line-broadening in t_1 and cosine-squared windows in t_2 and t_3 following linear-prediction extrapolation by 30% in t_2 and mirror-image linear-prediction extrapolation (*31*) by 85% in t_3. The highly overlapped region in the upper part of panel A contains 16 of the 30 H2′–C2′ cross peaks in LZ2, none of which are sufficiently resolved for analysis. Of the seven well-resolved cross peaks labeled in panels B–D, only C6 gave useful data in the two-dimensional experiment.

no significant couplings to ^{31}P, and C4′ resonances, which are affected by two strong $^3J_{C4'P}$ couplings in A-form RNA, respectively (*12*). Unfortunately, the highly selective coherence transfer for the CT–HCCH–COSY experiment eliminates these peaks from the observed spectra. Since our RNA sample has a 3′-hydroxy terminus, the C2′–H2′ peak for C30 provides a useful control, with I_c/I_d indistinguishable from unity in all spectra. In addition, as discussed above, C2′–H2′ peaks in A-form helical regions show only very small couplings. Controls with large *J* coupling constants are more problematic in CT–HCCH–COSY; for RNA molecules with no gauche$^-$ ϵ rotamers, all peaks may have I_c/I_d close to 1. A valuable check on the experimental setup can be obtained by modifying the sequence of Fig. 2A so that the first free precession period on carbon is set to $1/J_{CC}$ rather than $1/2 * J_{CC}$, the C1′-selective pulses are omitted, and the indirect ^{1}H evolution (t_1) is not incremented. In this spectrum, peaks in the C4′–H4′ region are dramatically attenuated in the coupled versus the decoupled spectrum for LZ2 (data not shown). Thus, this 2D experiment provides a control with large *J* coupling constants for the 3D experiment.

The most important limitation to spin–echo difference experiments for measuring $^3J_{CP}$ is the loss of sensitivity due to transverse relaxation during the constant-time delay on C2′. For LZ2, comparison of 47- and 23.5-ms ^{1}H/^{1}H subspectra yields an approximate median T_2 for the C2′ resonances of 29 ms (data not shown). For this or longer relaxation times, the precision of the measurement is sufficient to define the rotamer (Table 1). For RNA molecules significantly larger than LZ2, or in cases of severe resonance broadening due to slow internal motion (for example, A17 or G24 in LZ2), much shorter T_2 values can lead to such low sensitivity that it is impossible to obtain precise enough data to define the torsion angle to a single rotamer. We note, however, that noncanonical gauche$^-$ ϵ values predict large $^3J_{C2'P}$ values that are best analyzed at a constant-time delay of 23.5 ms ($1/J_{CC}$), resulting in increased sensitivity. Thus, nonstandard ϵ angles, which would indicate an unusual conformation of the RNA, will be easier to analyze in larger RNAs than residues in A-form regions. In addition, recently developed techniques for taking advantage of the generally lower transverse relaxation rates of multiple-quantum coherence to improve sensitivity (*21–23*) may be applied to this experiment in a straightforward way by replacing the long C2′ precession period with precession on C2′-H2′ multiple-quantum coherence. In LZ2, this technique does not lead to substantial improvements in sensitivity, presumably due to evolution under $^3J_{H2'H3'}$ (data not shown). In larger molecules, however, the multiple-quantum version is likely to have substantial sensitivity advantages and may well extend the size range for which this technique is applicable.

The earlier CT–HSQC experiment on LZ2 also yielded data on C4′ resonances (*12*). Interpretation of these results is more problematic, however, since both $^3J_{C4'P(i+1)}$, related to ϵ, and $^3J_{C4'P(i)}$, related to the C4′–C5′–O5′–P (β) torsion angle, will affect the observed intensity ratio (*12*). Modification of the CT–HCCH–COSY experiment to include a carbon–carbon isotropic mixing sequence (*24, 25*), yielding spin-echo difference CT–HCCH–TOCSY spectra, should also yield data on C4′ resonances. However, the multiple $^3J_{C4'P}$ couplings can limit the use of these data in structure determination.

In conclusion, we have introduced an improved technique for measuring $^3J_{C2'P}$ coupling constants, which are directly related to ϵ torsion angles in RNA oligonucleotides. These experiments allow the analysis of over twice as many residues in our 30-nucleotide RNA as previous methods by virtue of the superior resolution of H1′ and C1′ resonances in RNA. Due to the greatly improved peak dispersion, the spin–echo difference CT–HCCH–COSY experiment is the method of choice for determining $^3J_{C2'P}$ values in larger RNA oligomers.

TABLE 1
$^3J_{C2'P}$ Coupling Constants (in Hz) in LZ2

Residue	47-ms (CT–C2′) CT–HCCH–COSY	47-ms (CT–C1′) CT–HCCH–COSY	44-ms CT–HSQC[a]	ϵ rotamer[b]
G1	2.0–4.6	ca. 0	≤3.6[c]	t
C2	0.8–3.1	ca. 0	Overlap	t
G3	Overlap	≤1.8	Overlap	t
A4	≤2.2	≤0.8	Overlap	t
C5	≤0.8	≤2.8	Overlap	t
C6	≤1.4	≤3.4	≤2.3	t
G7	Too weak[d]	≤9.1	Overlap	nd
A8	3.4–6.9	≤3.6	Overlap	nd
G9	≤5.4	nd[e]	2.1–5.1	nd
C10	ca. 0	≤2.1	Overlap	t
C11	≤2.5	0.4–3.2	Overlap	t
A12	≤1.0	≤2.9	1.4–4.9	t
G13	ca. 0	Overlap	Overlap	t
C14	≤2.1	≤2.7	≤2.5	t
G15	≤2.6	≤2.7	≤2.3	t
A16	3.2–6.3	Too weak	≤3.4	nd
A17	2.8–8.6	≤8.7	≤5.4[c]	nd
A18	0.8–2.9	≤2.6	≤3.9	t
G19	2.4–5.0	3.4–6.6	≤2.5	nd
U20	≤2.5	1.0–3.3	≤3.3	t
U21	ca. 0	2.3–4.1	Overlap	t
G22	Overlap	1.1–4.2	Overlap	t
G23	1.7–3.3	Overlap	Overlap	t
G24	4.1–8.5	3.0–9.2	Overlap	nd
A25	ca. 0	≤2.7	≤3.1	t
G26	≤2.7	≤2.0	Overlap	t
U27	Overlap	Overlap	Overlap	nd
C28	Overlap	Overlap	Overlap	nd
G29	ca. 0	0.9–2.7	Overlap	t

Note. Analysis of experimental error using data from A-form residues (see text) inherently results in a subset of such residues yielding nonphysical negative coupling values; these values are reported as ''ca. 0.''

[a] Values taken from Legault *et al.* (*12*), listed for comparison.

[b] Rotameric state for ϵ torsion angle determined from the CT–HCCH–COSY spectra (see text).

[c] Taken from analysis of the 22-ms CT–HSQC spectra (*12*).

[d] Peak too weak for reliable quantitation.

[e] Nd means the peak was not analyzed due to conflict with spectral artifact.

ACKNOWLEDGMENTS

This work was supported by NIH Grants AI30762 and AI33098 to A.P. and a Helen Hay Whitney Foundation Postdoctoral Fellowship to C.G.H. The authors thank the Colorado RNA Center for support of RNA research on the Boulder campus and Dr. Pascale Legault for providing the lead-dependent ribozyme sample.

REFERENCES

1. K. Wüthrich, ''NMR of Proteins and Nucleic Acids,'' Wiley, New York (1986).
2. S. S. Wijmenga, M. M. W. Mooren, and C. W. Hilbers, *in* ''NMR of Macromolecules: A Practical Approach'' (G. C. K. Roberts, Ed.), pp. 217–288, Oxford Univ. Press, Oxford, UK, 1993.
3. A. Pardi, *Methods Enzymol.* **261,** 350–380 (1995).
4. G. Varani, F. Aboul-ela, and F. H.-T. Allain, *Prog. Nucl. Magn. Reson. Spectrosc.* **29,** 51–127 (1996).
5. H. Schwalbe, J. P. Marino, G. C. King, R. Wechselberger, W. Bermel, and C. Griesinger, *J. Biomol. Nucl. Magn. Reson.* **4,** 631–644 (1994).
6. H. Schwalbe, W. Samstag, J. W. Engels, W. Bermel, and C. Griesinger, *J. Biomol. Nucl. Magn. Reson.* **3,** 479–486 (1993).
7. C. Griesinger, O. W. Sørensen, and R. R. Ernst, *J. Chem. Phys.* **85,** 6837–6852 (1986).
8. H. Schwalbe, J. P. Marino, S. J. Glaser, and C. Griesinger, *J. Am. Chem. Soc.* **117,** 7251–7252 (1995).
9. J. P. Marino, H. Schwalbe, S. J. Glaser, and C. Griesinger, *J. Am. Chem. Soc.* **118,** 4388–4395 (1996).
10. G. W. Vuister, S. Grzesiek, F. Delaglio, A. C. Wang, R. Tschudin, G. Zhu, and A. Bax, *Methods Enzymol.* **239,** 79–105 (1994).
11. G. W. Vuister, A. C. Wang, and A. Bax, *J. Am. Chem. Soc.* **115,** 5334–5335 (1993).
12. P. Legault, F. M. Jucker, and A. Pardi, *FEBS Lett.* **362,** 156–160 (1995).
13. T. Pan and O. C. Uhlenbeck, *Biochemistry* **31,** 3887–3895 (1992).
14. T. Pan and O. C. Uhlenbeck, *Nature* **358,** 560–563 (1992).
15. T. Pan, B. Dichtl, and O. C. Uhlenbeck, *Biochemistry* **33,** 9561–9565 (1994).
16. P. Legault and A. Pardi, *J. Am. Chem. Soc.* **116,** 8390–8391 (1994).
17. P. Legault, ''Structural Studies of Ribozymes by Heteronuclear NMR Spectroscopy,'' Ph.D. thesis, University of Colorado, Boulder (1995).
18. L. E. Kay, M. Ikura, and A. Bax, *J. Am. Chem. Soc.* **112,** 888–889 (1990).
19. S. Grzesiek and A. Bax, *J. Am. Chem. Soc.* **114,** 6291–6293 (1992).
20. E. P. Nikonowicz, A. Sirr, P. Legault, F. M. Jucker, L. M. Baer, and A. Pardi, *Nucl. Acids Res.* **20,** 4507–4513 (1992).
21. S. Grzesiek, H. Kuboniwa, A. P. Hinck, and A. Bax, *J. Am. Chem. Soc.* **117,** 5312–5315 (1995).
22. S. Grzesiek and A. Bax, *J. Biomol. Nucl. Magn. Reson.* **6,** 335–339 (1995).
23. J. P. Marino, J. L. Diener, P. B. Moore, and C. Griesinger, *J. Am. Chem. Soc.* **119,** 7361–7366 (1997).
24. S. W. Fesik, H. L. Eaton, E. T. Olejniczak, E. R. P. Zuiderweg, L. P. McIntosh, and F. W. Dahlquist, *J. Am. Chem. Soc.* **112,** 886–888 (1990).
25. A. Bax, G. M. Clore, and A. M. Gronenborn, *J. Magn. Reson.* **88,** 425–431 (1990).
26. B. A. Messerle, G. Wider, G. Otting, C. Weber, and K. Wüthrich, *J. Magn. Reson.* **85,** 608–613 (1989).
27. A. Bax and S. S. Pochapsky, *J. Magn. Reson.* **99,** 638–643 (1992).
28. D. Marion, M. Ikura, R. Tschudin, and A. Bax, *J. Magn. Reson.* **85,** 393–399 (1989).
29. H. Geen and R. Freeman, *J. Magn. Reson.* **93,** 93–141 (1991).
30. A. J. Shaka, P. B. Barker, and R. Freeman, *J. Magn. Reson.* **64,** 547–552 (1985).
31. G. Zhu and A. Bax, *J. Magn. Reson.* **90,** 405–410 (1990).